Preprint Title Temperature and chemical effects on the interfacial energy between Ga-In-Sn eutectic liquid alloy and nano-asperities

Authors Yujin Han, Pierre-Marie Thebault, Corentin Audes, Xuelin Wang, Haiwoong Park, Jian-Zhong Jiang and Arnaud Caron

Publication Date 23 Feb. 2022

Article Type Full Research Paper

ORCID® iDs Yujin Han - https://orcid.org/0000-0001-7166-3029; Arnaud Caron - https://orcid.org/0000-0003-0985-7441

Temperature and chemical effects on the interfacial energy between Ga-In-Sn eutectic liquid alloy and nano-asperities

Yujin Han,[1] Pierre-Marie Thebault,[1,2] Corentin Audes, [1,2] Xuelin Wang,[3] Haiwoong Park,[1] Jian-Zhong Jiang*[3] and Arnaud Caron*[1]

Address: [1] KOREATECH – Korea University of Technology and Education, School of Energy, Material and Chemical Engineering, Cheonan, 31253 Republic of Korea, [2]UTT – University of Technology Troyes, 1004 Troyes, France, and [3]International Center of New-Structured Materials (ICNSM), Laboratory of New-Structured Materials, State Key Laboratory of Silicon Materials, School of Materials Science and Engineering, Zhejiang University, Hangzhou, 310027, People's Republic of China

Email: Arnaud Caron – arnaud.caron@koreatech.ac.kr; Jian-Zhong Jiang – jiangjz@zju.edu.cn

* Corresponding authors

Abstract

The interfacial energies between eutectic Ga-In-Sn liquid alloy and single nanoscopic asperities of SiO_x, Au, and PtSi have been determined in the temperature range between room temperature and 90 °C by atomic force spectroscopy. For all asperities used here, we find that the interfacial tension of eutectic Ga-In-Sn liquid alloy is smaller than its free surface energy by a factor of two (for SiO_x) to eight (for PtSi). Any significant oxide growth upon heating studied here was not detected and the

measured interfacial energies strongly depend on the chemistry of the asperities. We also observe a weak increase of the interfacial energy as a function of the temperature, which can be explained by the reactivity between SiO_x and Ga and the occurrence of chemical segregation at the liquid alloy surface.

Keywords

Liquid alloy; interfacial energy; AFM

Introduction

Recently, room temperature liquid Ga-based alloys are attracting interest from various scientific communities, involving chemical [1], biomimetic [2], microfluidic [3], electrical [4], and materials science [5]. This increased interest owes to the low viscosity, high thermal, and electrical conductivity of these alloys, on the one hand, and their non-toxicity and low vapor pressure on the other hand. Room temperature liquid Ga-based alloys are considered materials for direct writing and printing stretchable and flexible electronic devices, such as antennas or wires [5-7]. Such applications and the related processing of liquid metals strongly depend on their surface and interfacial properties. The surface tension of room temperature liquid Ga-based alloys has been reported to be lowered by a thin surface oxide layer [8]. In Ref. [9], the authors electrochemically controlled the growth and removal of gallium oxide to tune the surface tension of liquid gallium. Oxygen is a surface-active substance, and its effect on surface tension has been investigated for various liquid metals [10]. In metallic alloys, surface segregations have also been observed, where an element with a higher oxygen affinity enriches at the surface to form an oxide [10]. This effect has also been used to trigger the reaction of thin oxide films at the liquid-vapor interface with liquid gallium alloys [11]. While the

liquid-vapor interface of liquid gallium-based alloys has been well investigated, the wetting of liquid gallium alloys on different substrates has not yet attracted as much attention. Recently, authors in Ref. [12] highlighted the role of the oxide skin on the adhesion strength of gallium-based alloys on various substrates. Specifically, the authors found that the resulting adhesion strength is low when the oxide skin surrounding a liquid drop is not disrupted during application onto a substrate.

In contrast, when the oxide skin breaks, new oxide reforms at the solid-liquid interface with a substrate, which results in adhesion. Also, the wetting of liquid Ga-In alloy has been related to gallium's adsorption energy on three different substrates (steel, gold, and Al) [13]; with the wetting becoming better as the adsorption energy of gallium onto the substrate becomes more negative. In the case of Fe and Cu substrates, it was observed that liquid gallium reacts with the substrate to form an intermetallic layer at the gallium-substrate interfaces, which promotes the wetting of the gallium melt [14, 15]. Similarly, room temperature liquid eutectic Ga-In and eutectic Ga-In-Sn alloys have been reported to reactively wet thin indium and tin foils [16]. In Ref. [16] also, the authors demonstrated that the wetting of the same liquid alloys could be tuned by texturing the substrate surface.

The wetting of gallium-based liquid alloys is thus complex and depends on the stability of the oxide at the liquid-substrate interface, the reactivity with the substrate material, and the substrate topography. In this work, we applied atomic force spectroscopy to determine the interfacial energy between eutectic Ga-In-Sn liquid alloy and single nanoscopic asperities of SiO_x, Au, and PtSi in the temperature range between room temperature and 90 °C. The choice of the asperity materials was motivated by their relevance in electronics and micro-/nanotechnology. The surface chemical composition of the liquid alloy was measured by x-ray photoelectric spectroscopy before and after heating to 100

°C for three hours. Furthermore, we imaged the nanoscopic asperities after measurements on the metallic liquid alloy by SEM to evidence possible liquid residues. For all asperities used in this work, we find that the interfacial tension of eutectic Ga-In-Sn liquid alloy is smaller than its free surface energy by a factor of two (for SiO_x) to eight (for PtSi). While we did not observe any significant oxide growth upon heating, the measured interfacial energies strongly depend on the chemistry of the asperities. Furthermore, we observe a weak increase of the interfacial energy as a function of the temperature. We discuss our results based on the reactivity between SiO_x and Ga and the occurrence of chemical segregation at the liquid alloy surface.

Materials and experimental methods

We prepared a eutectic Ga-In-Sn liquid alloy by melting the mixture of its solid constituents with the composition of 78.8 at.% Ga, 13.2 at.% In, and 8 at.% Sn, whose melting point is approximately 283 K [17]. We measured the interfacial tension between Ga-In-Sn liquid eutectic alloy and atomic force microscopy (AFM) tips of different chemistries as a function of the temperature (T = 21 °C – 90 °C) by AFM force spectroscopy using an XE100 AFM equipped with a heating stage (manufactured by Park Instruments, Republic of Korea). We recorded force-distance curves with PtSi-coated Si cantilevers (PtSi-cont, manufactured from NanoSensors, Switzerland), SiO_x cantilevers (contsc, manufactured from NanoSensors, Switzerland), and Au-coated Si cantilevers (contscAu, manufactured from NanoSensors, Switzerland). Before measurements, the sensitivity of the AFM photodiode was calibrated by recording a force-distance curve with each cantilever on a quartz glass sample (manufactured by Goodfellow, United Kingdom) and extracting its slope in the range of repulsive forces.

Subsequently, we determined the bending stiffness C_n of each cantilever by analyzing its thermal noise vibration [18]. After measurements, each tip was investigated by SEM about possible material transfer from the liquid alloy sample and to determine its half-opening angle θ. Table 1 summarizes the properties of the cantilevers used in this work.

Table 1: Cantilevers' properties

	PtSi-Cont	Contsc	ContscAu
C_n [N/m]	0.24	1.14	0.89
θ [°]	12.5	5	12.5

Force spectroscopy measurements consisted of approaching a cantilever towards the sample's surface at varying velocity $\frac{dZ}{dt}$ = 0.1 – 25 μm/s (see Figure 1). We repeated force spectroscopy measurements at each approach/retraction velocity 15 times.

We used the approach part of the curves to calculate the force-penetration curves according to $\delta = Z - \frac{F_n}{C_n}$. The determination of the interfacial energy γ between an AFM tip and metallic liquid alloy is based on a balance between the pressure applied by the tip onto the liquid surface and the restoring pressure due to the line tension at the liquid interface, i.e., $p(\delta) = \frac{F_n(\delta)}{A(\delta)} = \frac{\gamma}{P(\delta)}$, where $A(\delta)$ is the contact area and $P(\delta)$ is the perimeter between tip and liquid. Assuming a conical shape for an AFM tip, the perimeter $P(\delta)$ and the contact area $A(\delta)$ can be expressed as $P(\delta) = 2\pi\delta \tan\theta$ and $A(\delta) = \pi\delta^2 \tan\theta \sqrt{1 + \tan^2\theta}$, where θ is the half opening angle of the tip, which we determined by scanning electron microscopy. We determined the interfacial energy *g*

between tip and liquid sample by fitting the function $F_n(\delta) = \frac{A(\delta)\gamma}{P(\delta)} = \gamma \frac{\sqrt{1+\tan^2\theta}}{2}\delta$ to our experimental data.

The chemical composition of a eutectic Ga-In-Sn liquid alloy sample was determined by x-ray photoelectronic spectroscopy (XPS) before and after heating in air at 100 °C for three hours. The spectrograms were recorded with a K-alpha$^+$ XPS system, manufactured by ThermoFischer Scientific, USA. Thereby, we used a monochromated Al K_α source and a spot size of 400 μm. The results presented below consist of the average of ten consecutively recorded measurements.

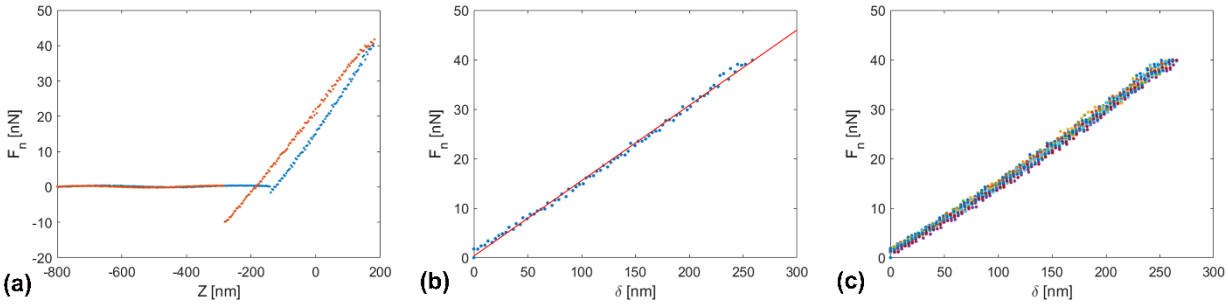

Figure 1: (a) Typical force-distance $F_n(Z)$-curve recorded with a SiO_x-tip on eutectic Ga-In-Sn melt at room temperature; the blue markers indicate the approach part, while the orange markers indicate the retraction part. (b) Force-penetration $F_n(\delta)$-curve, calculated from the approach part of the $F_n(Z)$-curve in (a), and its corresponding fit in red. (c) Superposition of 15 $F_n(\delta)$-curves recorded under the same conditions, i.e., temperature and approach velocity.

Results and Discussion

Figure 2 shows the temperature and velocity dependences of the interfacial energy between eutectic Ga-In-Sn melt and three AFM-tips of different chemistries: SiO_x, PtSi, and Au. For each dZ/dt-values, the temperature dependence of γ was fitted with the linear function $\gamma(T) = \gamma_m + \kappa(T - T_m)$, where γ_m is interfacial at the melting point, κ is

the temperature sensitivity of γ and T_m is the melting point of eutectic Ga-In-Sn melt. The values of γ_m and κ are also shown as a function of dZ/dt in Figure 2. For all three tips, we observe slight increases of γ with the temperature. $\gamma(T)$ significantly depends on the tip chemistry: γ_m and κ are lowest for PtSi-tips and increase in the order of Au-tip and SiOx-tip. However, these values do not appear to depend on the approach velocity of the tips toward the liquid sample. Table 2 indicates the average values of γ_m and κ and their ranges for the three different tip chemistries. Specifically, we find $\overline{\gamma_m}$ = 230 mN/m and $\bar{\kappa}$ = 3 mN/Km for SiOx, $\overline{\gamma_m}$ = 110 mN/m and $\bar{\kappa}$ = 2 mN/Km for Au, and $\overline{\gamma_m}$ = 68 mN/m and $\bar{\kappa}$ = 0.8 mN/Km for PtSi.

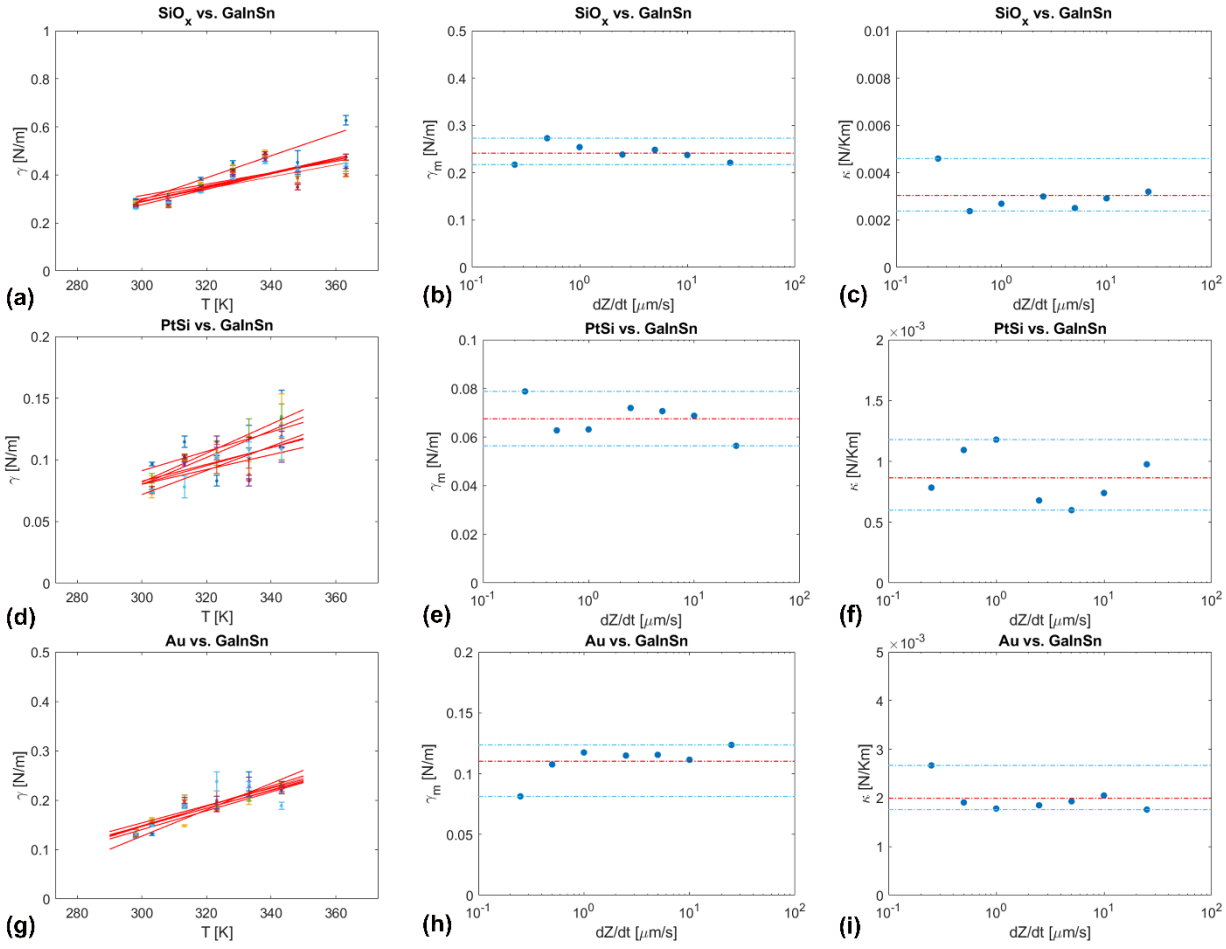

Figure 2: (a, d, g) Interfacial energy γ as a function of the temperature determined with dZ/dt = 0.25 – 25 mm/s; (b, e, h) interfacial energy at the melting point γ_m as a

function of d*Z*/d*t* (the mean value of γ_m is indicated as a red dashed line and the range of values is indicated by two blue dashed lines); (c, f, i) temperature sensitivity κ of the interfacial energy as a function of d*Z*/d*t* (the mean value of κ is indicated as a red dashed line and the range of values is indicated by two blue dashed lines).

The surface tension of Ga-In-Sn eutectic liquid alloy at the melting point has been reported to be γ_m^* = 587 mN/m, while its temperature sensitivity is κ^* = -10 mN/Km [19]. Expectedly, this value for the surface energy is larger than the interfacial energy values determined in this work. However, the positive κ-values determined in this work are unexpected and require a thorough discussion. In the following, we also discuss the effect of tip chemistry and oxide growth on the interfacial energy of Ga-In-Sn.

Table 2: Average and range of γ- and κ-values for PtSi, SiO_x, and Au tip materials.

	PtSi	SiO_x	Au
$\overline{\gamma_m}$ [mN/m]	68	230	110
$\bar{\kappa}$ [mN/Km]	0.8	3	2

The measurements presented here were performed in air. It is thus likely that a thin native oxide layer, which may have further grown upon heating, affected our measurements. Figure 3 and Table 3 show XPS results obtained on a drop of Ga-In-Sn eutectic liquid before and after heating in air at 100 °C for three hours. The choice of this duration roughly corresponds to the time necessary to complete a series of AFM measurements.

From Figure 3 and Table 3, it appears that after heating, the oxygen concentration at the surface of Ga-In-Sn eutectic liquid slightly decreased. Note that the 1s orbital of

oxygen indicates the presence of carbonate groups at the surface of the Ga-In-Sn eutectic melt. Similarly, and not shown here, we observed a signal corresponding to the 1s orbital of carbon. We attribute these contributions (CO_3^{2-}, C-C/C-H, and C-O) to contamination from the ambient. As mentioned above, we performed the XPS measurements on these liquid samples without any prior Ar^+-ion sputtering or any further heating inside the vacuum chamber of the XPS instrument.

Given that these contributions arose from contamination by the ambient, we excluded them from our calculations of the surface chemical composition. From Figure 3, one can further recognize that the melt's surface oxide mainly consists of gallium and tin oxides, with a minor contribution from indium oxide. After heating at 100 °C for three hours, this general trend was preserved.

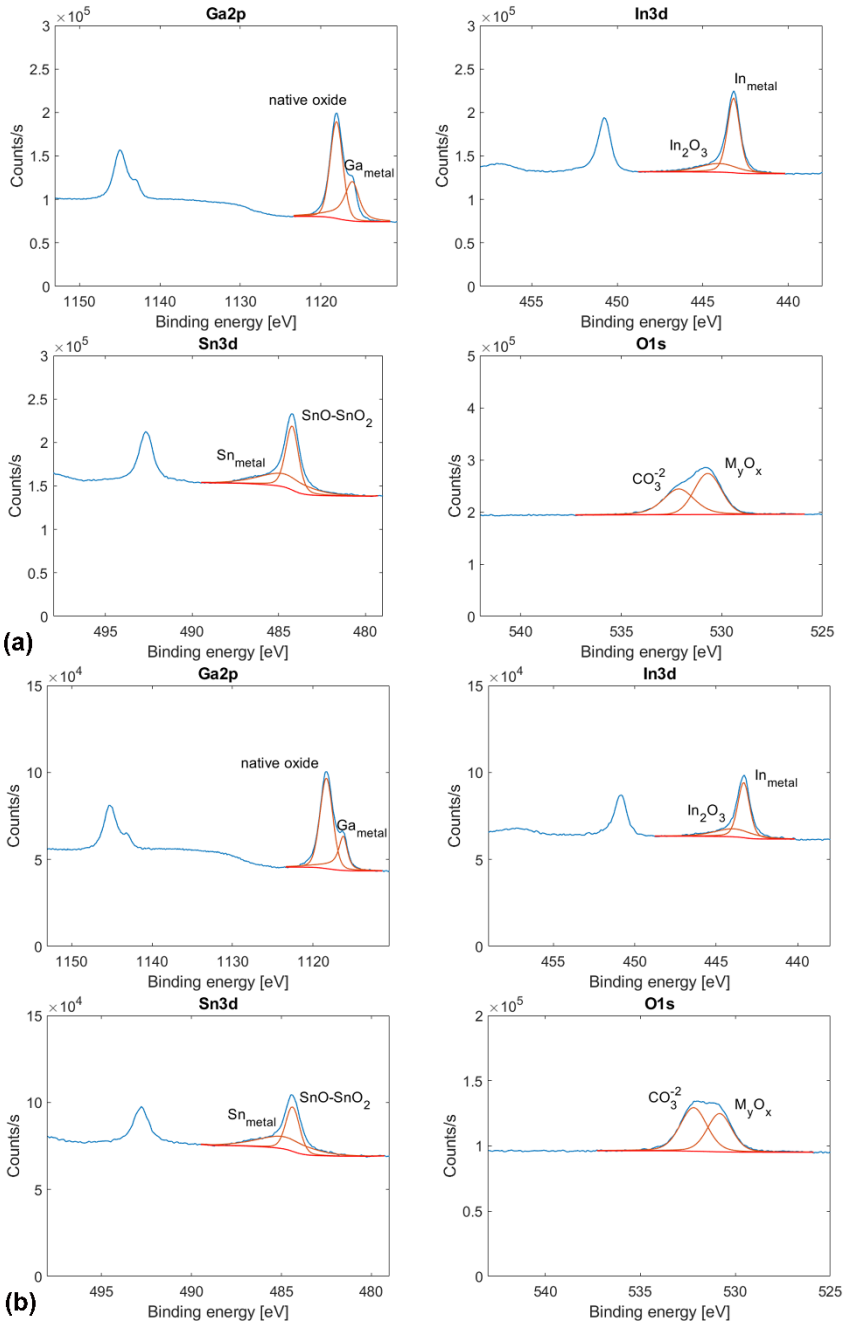

Figure 3: XPS results for eutectic Ga-In-Sn melt (a) before and (b) after heating at 100 °C for three hours.

From Table 3, it appears that after heating, the oxygen concentration at the surface of Ga-In-Sn eutectic liquid slightly decreased, i.e., from 53.7 at% to 49.9 at%. Moreover, the atomic fraction of gallium bounded as a native oxide increased from 23.2 at% to 27.0 at%, while the atomic fractions of tin and indium bounded as oxides (SnO or SnO_2,

and In_2O_3) did not significantly change. Given the atomic concentrations in Table 3, the native mixed surface oxide of the Ga-In-Sn eutectic liquid consists of GaO_2-Sn_2O_3-In_2O_3 or $(Ga_{0.8}Sn_{0.14}In_{0.06})O_2$. After heating, this concentration changed to $(Ga_{0.84}Sn_{0.10}In_{0.06})O_2$. The enrichment of the surface oxide in gallium at the expense of oxygen may indicate that oxygen was brought into solution in the Ga-In-Sn bulk liquid during heating.

Further, we estimate the change of the surface oxide thickness based on the Ganative oxide/Gametal-ratio change. Before heating, we calculate this ratio to be 2.38, while after heating, we find 2.64. The slight increase in the $Ga_{native\ oxide}/Ga_{metal}$-ratio after heating indicates that the surface oxide thickness did not significantly increase if we consider the oxide enrichment in Ga. According to the manufacturer, the interaction depth of the XPS was ~10 nm. We detected metallic bonded Ga, In, and Sn, thus we infer that the oxide layer was less than 10 nm thick. The thickness and composition of the surface oxide of a similar newly developed Ga-In-Sn-Zn liquid alloy have been characterized by TEM and XPS [20]. There, the authors reported on the effect of electron beam exposition time on the growth of a $ZnGa_2O_4$ layer. After 35 min irradiation, the oxide layer had grown from 2 nm to less than 5 nm. Besides this moderate growth, the authors observed the partial crystallization of the oxide layer during electron beam exposition. Our results on the temperature dependence of the interfacial energy between Ga-In-Sn eutectic liquid and AFM-tips were performed by dipping AFM tips inside a Ga-In-Sn liquid drop. The penetration depth of the tips was in the order of several 100 nm.

We did not observe any pop-in in the force-penetration curves that would indicate a sharp rupture event of the oxide film. Such an observation required a higher sampling rate than used during measurements. However, the experimental data points deviate from the linear fit function at penetration depth values below 50 nm (see figure 2(b, c)).

We attribute this deviation to the deformation of the liquid-supported oxide film up to its breakthrough. The penetration of the tip at larger depths is thus expected to be representative of the nano-asperities/metallic melt contact.

Furthermore, we estimated the chemical composition of the metallic melt below the oxide layer from the concentrations listed in Table 3. In the case of as-received Ga-In-Sn eutectic liquid, we find $Ga_{55.38}In_{28}Sn_{16.62}$, while after heating, we find $Ga_{56.75}In_{24.61}Sn_{18.64}$. Both compositions strongly deviate from the nominal composition of the alloy $Ga_{78.8}In_{13.2}Sn_{8}$. These results hint at chemical segregations at the metallic liquid surfaces, whose net effect is to reduce the surface tension of the liquid alloy (see discussion below).

Table 3: Surface chemical composition of Ga-In-Sn eutectic melt (a) before and (b) after heating for three hours at 100 °C.

	Ga_{metal}	$Ga_{native\ oxide}$	In_{metal}	In_{In2O3}	Sn_{metal}	$Sn_{SnO-SnO2}$	O_{MyOx}
As received	9.7	23.2	4.9	1.7	2.9	3.9	53.7
After heating at 100 °C	10.2	27.0	4.4	2.0	3.3	3.2	49.9

To discuss the effect of tip chemistry and temperature on our results, it shall be convenient to remind the reader about the physical origin and the thermodynamic interpretation of the surface and interfacial energies. The surface tension arises from the imbalanced bonding of atoms at the liquid/vapor interface: interfacial atoms are attracted by atoms in the bulk liquid to experience a pulling force in the direction from the surface to the bulk of the liquid. This effectively results in the tendency of the system to minimize its interfacial area with vapor or a vacuum. Hence, the surface tension can

be defined as the work to create a new unit area of surface reversibly. For a single component liquid, this translates as $\gamma^* A = F_s$, where *A* is the surface area and F_S is the Helmholtz free energy of the surface. In the case of a multi-components and single-phase liquid, this equality is reduced by chemical segregation at the surface, i.e., $\gamma^* A = F_s - \sum_i \mu_i \Gamma_i$, where μ_i is the chemical potential of the i^{th} component and Γ_i is its adsorption [21]. Neglecting the effect of surface segregation on the surface tension, the differential of the Helmholtz free energy of the surface can be written as $dF_s = \gamma^* dA + A d\gamma^*$ or $dF_s = \gamma^* dA + A\left(\frac{\partial \gamma^*}{\partial T}\right)_A dT$, which allows a correlation of the thermal sensitivity of the surface or interfacial tension $\kappa = \frac{d\gamma}{dT}$ with the surface or interfacial entropy $S_s = -A\left(\frac{\partial \gamma}{\partial T}\right)_A$.

The surface tension of Ga-In-Sn eutectic liquid at the melting point has been reported to γ_m^* = 587 mN/m. Since the surface tension originates from the bonding unbalance of atoms at the liquid/vapor interface [22], it shall be no surprise that the interfacial tension of the same liquid in contact with a solid is smaller since a solid surface also consists of atoms with unsaturated bonds that can minimize their energy by bonding with atoms from the liquid surface. Depending on the chemistry of the AFM tip, we find that a factor of two to eight reduces the interfacial energy compared to the surface energy. Figure 4 shows SEM images of the tips after measurements on the Ga-In-Sn eutectic liquid. Unlike the PtSi- and Au-tips, the SiO_x-tip in Figure 4 exhibits residues of the liquid alloy up to a height from the tip apex $h \approx 200$ nm that corresponds to the penetration depth of the tip into the liquid alloy. Coincidently, we determined the largest interfacial tension value at the melting point of the liquid alloy for the same tip, $\overline{\gamma_m^{SiO_x}}$ = 230 mN/m. The adhesion of melt residues at the SiO_x tip can be attributed to the respective stabilities of the oxides at the tip and at the liquid surface, respectively.

Their stability can be discussed based on their respective melting points and enthalpies of fusion ΔH_{fus} and formation at T = 298.15 K $\Delta_f H^0_{298\,K}$. For amorphous SiO_2, the following values were reported: $T_m^{SiO_2}$ = 1726 K, $\Delta H_{fus}^{Sio_2}$ = 7.438 kJ/mol, and $\Delta_f^{SiO_2} H^0_{298\,K}$ = -910.68 kJ/mol [23]. For Ga_2O_3, the literature reports $T_m^{Ga_2O_3}$ = 2080 K, $\Delta H_{fus}^{Ga_2o_3}$ = 99.77 kJ/mol, and $\Delta_f^{Ga_2o_3} H^0_{298\,K}$ = -1090.85 kJ/mol [23]. Hence, it appears that Ga_2O_3 is significantly more stable than SiO_2, and we suggest that upon penetrating the Ga-In-Sn eutectic melt, oxygen atoms at the tip surface react with Ga to form a solid Ga_2O_3 layer at the tip/melt interface. In this scope, the $\overline{\gamma_m^{SiO_x}}$ -value determined in this work may have been increased by the presence of a solid Ga_2O_3 layer at the tip/melt interface. Our interpretation is supported by recent calculations of the surface energy of Ga_2O_3 in Ref. [24]. Depending on the surface orientation, a range of values between 0.6 N/m and 2.98 N/m has been reported.

The $\overline{\gamma_m^{Au}}$- and $\overline{\gamma_m^{PtSi}}$-values determined in this work are significantly lower than γ_m^* and $\overline{\gamma_m^{SiO_x}}$. Due to its chemical inertness, the reactivity of PtSi and eutectic Ga-In-Sn melt can be ruled out. Also, reactions between gold and the constituting elements of the metallic melt are not expected. Solid gallium has very poor solubility for gold, and Ga forms a eutectic with $AuGa_2$ with a melting temperature of 491 °C. We thus exclude its formation during our experiment. However, the Ga-rich melt has a large solubility for Au.

For this reason, we assume that a small amount of gold dissolved in the metallic melt investigated here. However, the dissolution of Au should be small since it is thermally activated. In the current study, we could not observe any degradation of the Au tip nor measure traces of Au in liquid Ga-In-Sn. The phase diagram of the Au-In alloy system is similar to that of Au-Ga. However, the difference is that the eutectic formed between

In and $AuIn_2$ lays at 156 °C, higher than the maximum temperature applied during our measurements. Finally, the Au-Sn system shows no solubility of Au in Sn and exhibits a eutectic between $AuSn_4$ and Sn at 211 °C. A reaction between Au and Sn can thus be ruled out for our experimental conditions.

In Ref. [24], the authors calculated the surface energy of gold nanoparticles of different shapes. The authors found that the surface energy sharply increases for diameters smaller than 5 nm for spherical particles. In our experiments, the Au-tip apex can be considered a sphere with a radius R = 25 nm. According to Ref. [25], the surface energy of the gold tip can be assumed to be in the range γ_{Au}^{*} = 1.15 J/m^2 – 1.30 J/m^2. The surface energy of stochiometric PtSi(010) was calculated as a function of the number of (010)-planes below the surface [26]. A weak decrease in surface energy was observed upon increasing the number of planes. For a supercell consisting of 25 (010)-planes, the authors in Ref. [26] calculated for the surface energy of PtSi γ_{PtSi}^{*} = 1.71 J/m^2. It is thus remarkable that the higher the tip material's surface energy, the lower the interfacial energy between the tip and the Ga-In-Sn eutectic melt becomes. This result is in so far expected that forming a tip/liquid interface rids areal parts of the tip/vapor and the Ga-In-Sn eutectic melt/vapor interfaces and thus decrease the energy of the system: the larger the individual free surface energies, the larger the energetic gain upon the formation of an interface.

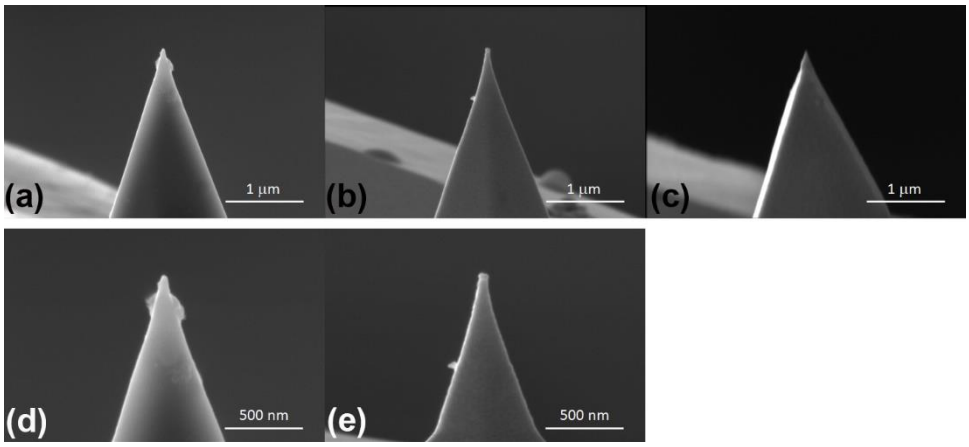

Figure 4: SEM images of the AFM tips used to collect the results presented in figure 2: (a, d) SiO_x tip, (b, e) Au-tip, and (c) PtSi tip.

Above, we have related the temperature sensitivity of the surface energy κ to the surface entropy S_s. For most liquids, the value κ is negative, owing to an increase in entropy at higher temperatures. This entropy increase can be rationalized by decreasing the coordination number at a liquid surface at higher temperatures. However, there are a few exceptions where κ has been observed to take positive values. For pure silver, a positive temperature sensitivity has been observed in the temperature range between 1200 K and 1500 K and associated with oxygen [10]. In that case, oxygen acts as a surface-active element that leads to chemical segregations at the surface. A similar phenomenon was reported for Ga-Bi liquid alloys, in which case a positive temperature sensitivity κ has been observed to increase with the bismuth content. The surface enrichment also explained this result in bismuth, which exhibits a lower surface tension than gallium. Our XPS results also hint at an enrichment in tin and indium at the surface of the Ga-In-Sn eutectic alloy. The surface tension of tin and indium at their melting point is γ_{Sn}^* = 689 mN/m and γ_{In}^* = 562 mN/m, while for pure gallium, the literature reports γ_{Ga}^* = 713 mN/m [27]. Thus, negative κ-values can be explained based on chemical surface segregations. In this line, we

suggest that the effect of tip chemistry on κ can be rationalized based on the solubility or reaction of the tip material with the metallic melt. We have already explained the high interfacial energy between SiO_x and the Ga-In-Sn eutectic melt based on the reaction of oxygen atoms from SiO_x with gallium atoms. This reaction is likely to be thermally activated, which would also explain the increase of the interfacial energy with the temperature based on the growth of an interfacial oxide layer. We suggest that tip material comes into solution in the Ga-In-Sn eutectic melt for the gold and platinum silicide tips. Though not verified here, we speculate that tip material's partial and thermally activated solubility in our metallic melt would form a segregation layer and increase the interfacial tension.

Conclusion

We have investigated the effect of temperature and chemistry on the interfacial energy between nanoscopic asperities of SiO_x, Au and PtSi, and Ga-In-Sn eutectic melt by atomic force spectroscopy. We find that the interfacial energy with Ga-In-Sn eutectic melt is a factor two to eight smaller than its surface tension for all asperities. We find that the interfacial energy is influenced by oxidation of the melt at the SiO_x/liquid metal alloy interface, which results in the largest interfacial energy measured in this work. In the case of gold and platinum silicide, the interfacial energy decreases in proportion to the surface energy of the tip material. Moreover, we observe a positive thermal sensitivity of the interfacial energy, which we explain based on chemical segregation at the interface with the Ga-In-Sn eutectic melt. Beyond the importance of our results for a comprehensive understanding of the physical chemistry of metallic melt

interfaces, these results are relevant for the design of a microfluidic system with metallic liquids governed by interfacial effects with the channel material.

Acknowledgments

Financial supports from the National Key Research and Development Program of China (2017YFA0403400), National Natural Science Foundation of China (11975202 and U1832203), and the Education and Research Promotion Program of Koreatech in 2020 are gratefully acknowledged.

References

1 Daeneke, T.; Khoshmanesh, K.; Mahmood, N.; de Castro, I.A.; Esrafilzadeh, D.; Barrow, S.J.; Dickey, M.D.; Kalantar-zadeh, K. Chem. Soc. Rev., **2018**, 47, 4073-4111.

2 Zhang, J.; Yao, Y.; Sheng, L.; Liu, J. Adv. Mater., **2015**, 27, 2648-2655.

3 Gao, Y.; Ota, H.; Schaler, E.W.; Chen, K.; Zhao, A.; Gao, W.; Fahad, H.M.; Leng, Y.; Zheng, A.; Xiong, F.; Zhang, C.; Tai, L.-C.; Zhao, P.; Fearing, R.S.; Javey, A. Adv. Mater., **2017**, 29, 1701985-1-8.

4 Hirsch, A.; Dejace, L.; Michaud, H.O.; Lacour, S.P. ACC. Chem. Res., **2019**, 52, 534-544.

5 Yang, C.; Bian, X.; Qin, J.; Guo, T.; Zhao, X. RSC Adv., **2014**, 4, 59541-59547.

6 Dickey, M.D. Adv. Mater., **2017**, 29, 1606425-1-19.

7 Boley, J.W.; White, E.L.; Chiu, G.T.-C.; Kramer, R.K. Adv. Funct. Mater., **2014**, 24, 3501-3507.

8 Khan, M.R.; Eaker, C.B.; Bowden, E.F.; Dickey, M.D. Proc. Natl. Acad. Sci. U.S.A., **2014**, 111, 14047-14051.

9 Chrimes, A.F.; Berean, K.J.; Mitchell, A.; Rosengarten, G.; Kalantar-zadeh, K. ACS Appl. Mater. Interf., **2016**, 8, 3833-3839.

10 Egry, I.; Ricci, E.; Novakovic, R.; Ozawa, S. Adv. Coll. Interf. Sci., **2010**, 159, 198-212.

11 Zavabeti, A.; Ou, J.Z.; Carey, B.J.; Syed, N.; Orrell-Trigg, R.; Mayes, E.L.H.; Xu, C.; Kavehei, O.; O'Mullane, A.P.; Kaner, R.B.; Kalantar-zadeh, K.; Daeneke, T. Science, **2017**, 358, 332-335.

12 Doudrick, K.; Liu, S.; Mutunga, E.M.; Klein, K.L.; Damle, V.; Varanasi, K.K.; Rykaczewski, K. Langmuir, **2014**, 30, 6867-6877.

13 Ding, Y.; Guo, X.; Qian, Y.; Xue, L.; Dolocan, A.; Yu, G. Adv. Mater., **2020**, 32, 2002577-1-8.

14 Cui, Y. ; Liang, F. ; Xu, S. ; Ding, Y. ; Lin, Z. ; Liu, J. Coll. Surf. A, **2019**, 569, 102-109.

15 Cui, Y.; Liang, F.; Yang, Z.; Xu, S.; Zhao, X.; Ding, Y.; Lin, Z.; Liu, J. ACS Appl. Mater. Interf., **2018**, 10, 9203-9210.

16 Kramer, R.K.; Boley, J.W.; Stone, H.A.; Weaver, J.C.; Wood, R.J. Langmuir, **2014**, 30, 533-539.

17 Wang, W.; Yu, Q.; Wang, X.; Dai, Z.; Cao, Q.; Reng, Y.; Zhang, D.; Jiang, J.-Z. J. Phys. Chem. C, **2021**, 125, 7413-7420.

18 Butt, H.J.; Jaschke, M. Nanotechnol., **1995**, 6, 1-7.

19 Plevachuk, Y.; Sklyarchuk, V.; Eckert, S.; Gerbeth, G.; Novakovic, R. J. Chem. Eng. Data, **2014**, 59, 757-763.

20 Yu, Q.; Zhang, Q.; Zong, J.; Liu, S.; Wang, X.; Wang, X.; Zheng, H.; Cao, Q.; Zhang, D.; Jiang, J. Appl. Surf. Sci., 2019, **492**, 143-149.

21 N.H. March, M.P. Tosi. Introduction to liquid state physics. World Scientific Press, Singapore (2002).

22Oriani, R.A. J. Chem. Phys., **1950**, 18, 575-578.

23Lamoreaux, R.H.; Hildebrand, D.L. J. Phys. Chem. Ref. Data, **1987**, 16, 419-443.

24Mu, S.; Wang, M.; Peelaers, H.; Van de Walle, C.G. APL Mater., **2020**, 8, 091105-1-6.

25Holec, D.; Dumitraschkewitz, P.; Vollath, D.; Fischer, F.D. Nanomaterials, **2020**, 10, 484-1-15.

26Niranjan, M.K. Surf. Sci., **2016**, 649, 27-33.

27Aqra, F.; Ayyad, A. Appl. Surf. Sci., **2011**, 257, 6372-6379.